

ene selectivities are consistent with homogeneous reactions in the absence of O<sub>2</sub>. Further experiments and simulation would be required to distinguish between these mechanisms.

This system is an example where extreme conditions can be used to produce a very high selectivity to a single product at high temperatures in a very efficient reactor configuration, even though thermodynamic equilibrium predicts mostly solid carbon and only a few percent ethylene. The process operates by combining the fast surface oxidation reactions on a modified Pt surface with homogeneous and heterogeneous dehydrogenation

processes. We have shown that homogeneous reactions alone cannot account for the observed results, but the specific role of homogeneous reaction steps, if any, has not yet been determined. We suggest that extreme conditions such as these may provide the environments to carry out similar reactions to produce chemicals with high efficiency, more efficient energy use, and less pollution.

#### References and Notes

1. Kirk-Othmer, *Encyclopedia of Chemical Technology* (Wiley, New York, 1991).
2. H. H. Kung, *Transition Metal Oxides: Surface Chemistry and Catalysis* (Elsevier, New York, 1989).

3. *Catal. Today* **157** (1997); A. Bielanski and J. Haber, *Oxygen in Catalysis* (Dekker, New York, 1991).
4. M. Huff and L. D. Schmidt, *J. Phys. Chem.* **77**, 11815 (1993).
5. C. Yokoyama, S. S. Bharadwaj, L. D. Schmidt, *Catal. Lett.* **38**, 181 (1996).
6. C. J. Astbury *et al.*, *U.S. Patent* **5**, 382, 741 (1995).
7. M. T. Paffett, S. C. Gebhard, R. G. Windham, B. E. Koel, *Surf. Sci.* **223**, 449 (1989); *J. Phys. Chem.* **94**, 6831 (1990).
8. E. Ranzi, T. Faravelli, P. Gaffuri, A. D'Anna, A. Ciajolo, *Combust. Flame* **108**, 24 (1997).
9. Partially supported by grants from NSF and the U.S. Department of Energy.

7 December 1998; accepted 18 March 1999

## Localization-Delocalization Transition in Quantum Dots

N. B. Zhitenev,<sup>1\*</sup> M. Brodsky,<sup>1</sup> R. C. Ashoori,<sup>1†</sup>  
L. N. Pfeiffer,<sup>2</sup> K. W. West<sup>2</sup>

Single-electron capacitance spectroscopy precisely measures the energies required to add individual electrons to a quantum dot. The spatial extent of electronic wave functions is probed by investigating the dependence of these energies on changes in the dot confining potential. For low electron densities, electrons occupy distinct spatial sites localized within the dot. At higher densities, the electrons become delocalized, and all wave functions are spread over the full dot area. Near the delocalization transition, the last remaining localized states exist at the perimeter of the dot. Unexpectedly, these electrons appear to bind with electrons in the dot center.

The problem of electron localization has remained a prime focus of experimental and theoretical research over the past 40 years. In 1958 Anderson (*1*) showed that, in one dimension and in the presence of an arbitrary disorder potential, an electron diffuses over only a finite length. A subsequent milestone in localization theory was the scaling hypothesis (*2*). A scaling law connects the properties of a system with the properties of its subsystems of smaller sizes. Scaling theory used conductivity as the only parameter needed to characterize a disordered system. This basic assumption originated from Thouless and Edwards (*3, 4*) and linked the dc conductivity of a finite disordered system with the sensitivity of electron energy levels to a modification of boundary conditions.

The dependence of a particular electronic state energy on boundary conditions reflects the probability density for an electron's wave function to reside at the boundary and thereby reveals the likelihood of permeating the bound-

ary. Despite all the success of the scaling theory, it is the theory developed for noninteracting systems. Here, we use Thouless's intuitively clear approach to localization to study the properties of a confined interacting electron droplet. We monitor how the energies to add single electrons to a quantum dot change as we vary the potential at the dot's edges.

In most quantum dot experiments (*5, 6*), a dot is weakly connected to two macroscopic leads. Applying a positive (negative) potential to a closely placed gate electrode increases (decreases) the number of electrons on the dot. At the particular gate potential at which an electron is added to the dot, the number of electrons on the dot can fluctuate by one, allowing single electrons to be added to the dot from one lead and to depart the dot through the other. The conductance through the dot displays a peak for these values of the gate voltage and remains zero for other values (*5, 6*). Note that if electrons cannot be transported through the dot, no conductance peak can be observed. Our method of single electron capacitance spectroscopy (SECS) displays a peak in the sample capacitance each time an electron is added to the dot (*7*). Because of the geometry (Fig. 1A) of our samples and because SECS measures charge rather than conductance, even electrons added to states localized within the dot are de-

tected in SECS measurements. SECS can thereby sense electrons even in dots that are electrically insulating. For high electron densities, both conductance and capacitance measurements yield similar results. Because of electron repulsion, more energy is required to add subsequent electrons to the dot. Charge in the dot behaves nearly as classical charge on a metallic disk, and electron additions appear nearly periodically with gate voltage (Coulomb blockade).

SECS measurements have shown (*7, 8*) that the low-density regime appears entirely different. Not only is the addition spectrum highly nonuniform, but peaks from subsequent electron additions can form pairs and bunches, apparently indicating that an unknown mechanism has eliminated the repulsive interaction between the two (or more) electrons. The pairing phenomenon arises both in large (>0.8- $\mu\text{m}$  diameter) disordered dots in which electrons are likely localized at random traps and in smaller (<0.5- $\mu\text{m}$  diameter) but more ordered dots. This investigation demonstrates that in the latter case the low-density system in quantum dots actually bifurcates into two subsystems: a central core and a periphery. The pairing phenomenon arises from an apparent and unexplained cancellation of the Coulomb repulsion between electrons in these two regions.

These dots are fabricated within an AlGaAs-GaAs heterostructure (Fig. 1A) described in (*7, 8*). The essential layers, from the substrate to the surface, are a conducting substrate of GaAs serving as the only contact lead to the dots, a AlGaAs tunnel barrier, an active GaAs layer where electrons are accumulated, and a blocking AlGaAs layer. On the top surface a small CrAu top gate was formed by electron beam lithography. This top gate was used as a mask for wet or reactive ion etching to completely deplete the active GaAs layer outside the covered region and therefore to produce the quantum dot below the top gate. Then a thin film of CrAu was evaporated over the formed structure. This film was thin enough to break at the edges of the previously fabricated top gate (*9*)

<sup>1</sup>Department of Physics and Center for Materials Science and Engineering, Massachusetts Institute of Technology, Cambridge, MA 02139, USA. <sup>2</sup>Bell Laboratories, Lucent Technologies, Murray Hill, NJ 07974, USA.

\*Present Address: Bell Laboratories, Lucent Technologies, Murray Hill, NJ 07974, USA.

†To whom correspondence should be addressed. E-mail: ashoori@mit.edu

and could be contacted separately (see schematic in Fig. 1A), serving as a side gate allowing repulsion of electrons from the edges of the dot through application of a negative potential.

In measuring the electron addition spectra of these dots, we first apply a large negative potential to the top gate,  $V_t$ , repelling all the electrons from the quantum dot. Then, we scan  $V_t$  toward more positive voltages, drawing the electrons back into the dot one by one. To detect the electron additions, we measure the ac capacitance between the top gate and

the contact layer at a frequency of 600 kHz. At  $V_t$  values corresponding to the electron additions, an electron oscillates between the dot and the contact responding to the small (about 60  $\mu\text{V}$ ) ac voltage and increasing the measured ac capacitance (7). In the example of the measured capacitance trace (Fig. 1C, left vertical panel), each peak (capacitance increases to the left) is a single electron contribution. The capacitance traces measured at different values of the side-gate potential  $V_s$  are plotted together on the gray-scale panels. The evolution of the addition energies with  $V_s$  can be easily perceived this way.

The electron addition energies are far less sensitive to the side-gate potential than to the top-gate potential, reflecting the difference in the geometrical capacitance. The field from the side gate decays strongly, moving toward the interior of the dot, because of the screening by bottom and top metal electrodes. Therefore, the slope of a peak as a function of  $V_s$  effectively measures the probability for an electron in the respective electronic state to reside at the periphery of the dot. At small electron numbers, the slope is small and varies strongly from peak to peak. Note that spacing in  $V_t$  also fluctuates strongly (10). The large fluctuations in peak spacing and slope indicate that electrons are localized and interact weakly with each other. On average, the slopes of traces increase with electron number and the spacing between traces decreases.

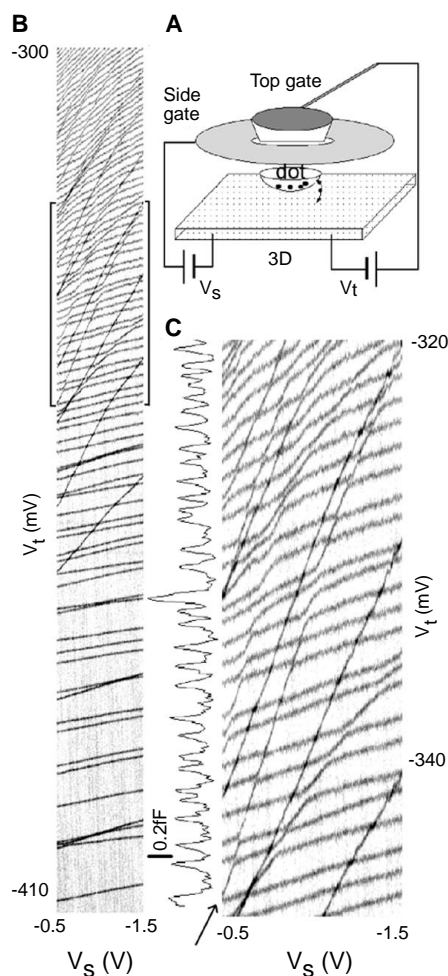


**Fig. 1.** (A) Schematic of quantum dot structure with side gate and scheme for application of bias voltages. (B) Gray-scale panel of measured capacitance with dark lines denoting capacitance peaks. Each peak corresponds to an electron addition to the dot. Top-gate voltage scale can be converted to the addition energy scale by multiplying by 0.5 (lever arm). Temperature, 50 mK. (C) Zoom in to part of (B) demarcated by brackets. Arrow points to a characteristic edge localized state. Line trace on the left shows a single experimentally measured capacitance trace as a function of top-gate voltage. Peaks arise from single electrons moving back and forth between the dot and the substrate in response to a small ac excitation. Panel was built from 250 separate capacitance traces.

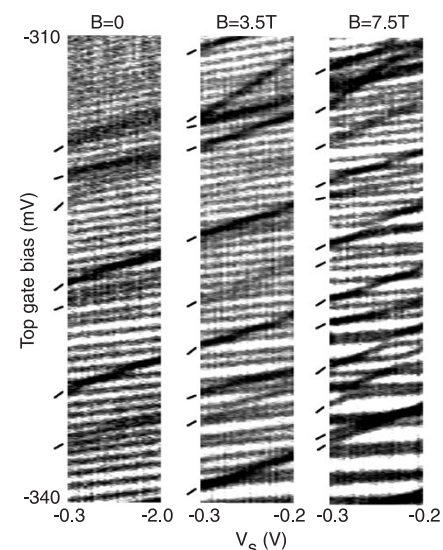


**Fig. 2.** Gray-scale panels demonstrating the effect of magnetic field on addition spectra. Temperature, 300 mK. At zero field most traces have only small slopes, indicating that most electrons are either delocalized throughout the dot or localized in the interior of the dot. As magnetic field increases, more states (dashes) appear with a steeper slope and are therefore confined to the dot periphery. Magnetic field thus appears to enhance localization of electrons into interior or periphery regions.

As more electrons are added to the dot, the electron droplet expands laterally. This increases the capacitance of the puddle to the surroundings and results in a decrease in the spacing as a function of  $V_t$ . The average lateral expansion also explains the increase in the coupling to the side gate and the increase of the slope. Above a critical density,  $n_c \sim 10^{11}\text{cm}^{-2}$  (about 100 electrons in the dot), corresponding to the top of the panel in Fig. 1B, the slopes of all electronic states become equal within the experimental resolution. Note that, for a perfectly metallic droplet in which all electronic states are similarly spread over the area of the dot, one expects equal slopes for all traces with  $V_s$  and precisely periodic electron additions as a function of  $V_t$  (Coulomb blockade).

The traces can be separated in two distinct groups with respect to their dependence on  $V_s$ . The presence of the traces with very large slopes is the most noticeable feature. The large capacitance to the side gate means that these states are mainly localized at the edge of the electron puddle. The traces of small slopes originate from electron additions to states with high probability density located near the dot center. We label them as interior states.

We now center our discussion on the intermediate range of electron density just before the delocalization transition, where most of the traces display nearly equal slope except for a few states with steeper slopes. Additional spectra at 300 mK from this region in another quantum dot were taken at several values of applied magnetic field (Fig. 2). Application of magnetic field perpendicular to the plane of the quantum dot strongly affects the addition spectrum. The general behavior of the addition spectrum as the dot evolves from localized to metallic-like with increasing density, appears qualitatively unchanged from the dot in Fig. 1B. The traces arising from the remaining states localized at the dot edge are indicated by tic marks in Fig. 2. The magnetic field breaks the regular metallic-like pattern of the addition spectrum and tends to localize electronic states at the center or at the periphery of the dot. This is clearly evidenced by the emergence of additional traces with large slope as the field strength is increased. Other traces display a diminished slope at increased fields, indicating that they arise from electronic states that have become localized near the center of the dot. Magnetic field effectively shifts the localization-delocalization transition toward higher numbers of electrons within the dot. Finally, note also that the traces at high fields are not always well separated as a function of  $V_t$ , as the Coulomb repulsion between electrons would ordinarily suggest. In fact, many traces appear clumped, similar to the bunching of levels observed in previous SECS experiments (8).

Figures 1B and 2 establish our ability to detect localization within the dot. We now focus on the interaction between electronic states localized at edge and center of the dot. Closer examination of Fig. 1B reveals that, upon increasing  $V_t$ , traces from states localized at the periphery traverse traces from states localized at the dot center. The splitting observed at these avoided crossings (anticrossings) is a measure of interaction between respective states. The presence of an electron in the lower state causes the additional energy of the crossing state to move up because of hybridization and the Coulomb repulsion between hybridized states. The lowest two of the edge localized (steep slope) states appear scarcely to interact with interior electron states at all. More interesting are the edge states that display noticeable interaction with other crossing states.

A typical trace from a periphery state (arrow in Fig. 1C) displays anticrossings with all the traces it traverses. The strength of the interactions fluctuates strongly over the range, with the splitting values varying by a factor of 5. Other localized states display similar strong fluctuations of the splitting values. On average, the splittings are smaller

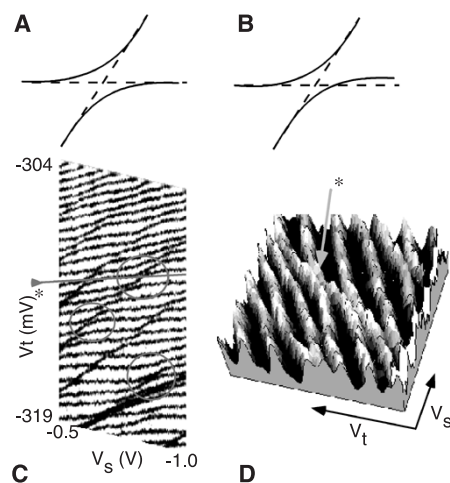


**Fig. 3.** (A) Sketch of the expected form for an anticrossing considering quantum mechanical and Coulomb interactions between electrons in different states. The chemical potential of  $(N + 1)$  electron state (left) is higher than or equal to the chemical potential of  $N$  electron state (right). (B) Sketch of an experimentally observed anomalous anticrossing; the chemical potential of  $(N + 1)$  electron state is lower than the chemical potential of  $N$  electron state. In this case, the removal of a periphery electron on the right-hand side of the diagram raises the chemical potential of the remaining  $N$  electrons facilitating the removal of another electron in the interior. (C) Top part of the addition spectrum from Fig. 1B skewed to level the traces of internal electrons. Some of the anomalous anticrossings are denoted by circles. (D) Surface map zooming in to the anomalous anticrossing marked by an asterisk. Energy levels clearly demonstrate the tendency of states to “stick” together at the anticrossing.

than the level spacing in the range shown. At higher electron number, the splittings grow to become comparable with the Coulomb blockade peak spacing, indicating an increased interaction between crossing states. Surprisingly, some very unusual anticrossing patterns can be seen here.

We zoom in on part of the addition spectrum immediately preceding the complete disappearance of patterns of anticrossings associated with localized states (Fig. 3C). To facilitate visualization, the image is skewed to compensate for the slope of the internal states. Intriguingly, at some of the anticrossings, the addition energy for the  $N$  electron state is higher than the addition energy for the  $(N + 1)$  electron state before the anticrossing (diagram in Fig. 3B). We note that all of the anticrossings at lower density shown in Fig. 1 follow a more typical pattern than in Fig. 3A.

The pattern of the interaction at lower density is generally consistent with the assumption that the localization of the periphery states is caused by strong fluctuations of the background potential. As more electrons are added to the dot, the interior puddle expands laterally and approaches a localized state at the periphery. This expansion appears to increase the interaction between the crossing states. Further, one may expect the interaction strength to be sensitive to the particular electron wavefunctions on both sides of the barrier. These may vary strongly, possibly accounting for the large fluctuation in the observed interactions. Examining a typical edge state (Fig. 1C, arrow), we see that the values of the anticrossing fluctuate by a factor of 5.

At higher electron density there are, however, a few features in the addition spectrum that appear inconsistent with the irregular single-particle localization by fluctuating potential. First, the last six localized states seen before the complete delocalization (in Fig. 1B) appear with nearly perfect periodicity in electron number. This observation is reproducible upon different thermal cyclings and was observed on many different quantum dots (8). Second, the localized edge states disappear above a critical density (determined by the top gate voltage) that is identical for many different quantum dots. Both observations indicate that the segregation results from electron correlations in a low-density electron droplet. We previously conjectured this hypothesis after having observed the periodic bunching in the addition spectra of quantum dots (8). This experiment visualizes directly the localized states confined to the perimeter of the dot.

A surprising observation is the unusual interaction between the edge localized and the bulk states. In this regime, the values of the splitting at the anticrossings grow to become comparable with the spacings in  $V_t$  for electrons entering the core. Therefore, the interaction

cannot be considered as a weak perturbation for the initial crossing states. If we focus on the vicinity of the anticrossing (Fig. 3D), this looks as though the removal of the edge electron from the system actually raises the chemical potential (by increasing the energy to add an electron to the system). This behavior suggests that there exists a mechanism for attraction between electrons in the crossing states overcoming the usual Coulomb repulsion. Indeed, the clear tendency for electron peaks to move closer to each other over an extended interval of  $V_s$  is seen, implying a possible energetic benefit of the paired configuration.

The exact physical mechanism of the segregation into an interior puddle and periphery localized states has yet to be established. We observe the segregation only at densities below a critical density of  $n_c = 1 \times 10^{11} \text{ cm}^{-2}$ . With the conventional parameter  $r_s = a_B^{-1}(\pi n_c)^{-1/2}$ , where  $a_B$  is the Bohr radius (about 100 Å in GaAs) to describe the interaction strength, this density corresponds to  $r_s \sim 1.8$ . This is far below the value of  $r_s \sim 8$  to 36 calculated for formation of the Wigner crystal (11), as well as below  $r_s \sim 8$  for recently observed two-dimensional (2D) metal-insulator transition for electrons in Si and holes in GaAs (12). However, this is the density range where Eisenstein *et al.* (13) experimentally observed the negative compressibility in a 2D electronic system. The physical essence of the negative compressibility is an overscreening of a probe electron by the correlated electron liquid. Recently, Levitov (14) demonstrated that the negative compressibility can result in a significant spatial oscillation of the density at the edge of the electron droplet. Whether such oscillation can result in the edge state localization remains unclear.

The striking pattern of the anticrossings shown in Fig. 3 suggests that, instead of usual repulsion of the electron states, there may exist an effective attraction between electrons in different localized regions. Experimentally, the manifestations of the pairing tendency were observed previously (7, 8) but, despite intensive theoretical efforts (15), the origin of the visible attraction is not yet understood.

#### References and Notes

1. P. W. Anderson, *Phys. Rev. B* **109**, 1492 (1958).
2. E. Abrahams, P. W. Anderson, D. C. Licciardello, T. V. Ramakrishnan, *Phys. Rev. Lett.* **42**, 673 (1979).
3. D. J. Thouless, *Phys. Rep.* **13**, 93 (1974).
4. J. T. Edwards and D. J. Thouless, *J. Phys. C* **5**, 807 (1972).
5. M. A. Kastner, *Phys. Today* **46**, 24 (1993).
6. R. C. Ashoori, *Nature* **379**, 413 (1996).
7. ——— *et al.*, *Phys. Rev. Lett.* **68**, 3088 (1992).
8. N. B. Zhitenev, R. C. Ashoori, L. N. Pfeiffer, K. W. West, *ibid.* **79**, 2308 (1997).
9. S. Tarucha, D. G. Austing, T. Honda, R. J. van der Hage, L. P. Kouwenhoven, *ibid.* **77**, 3613 (1996).
10. In our dots, the single-particle quantum level spacing is about 1/10th the charging energy; hence, the energy of spatial quantization cannot be the origin of the strong fluctuations of the addition spectrum.

11. A. G. Eguluz, A. A. Maradudun, R. J. Elliott, *Phys. Rev. B* **27**, 4933 (1983); S. T. Chui and B. Tanatar, *Phys. Rev. Lett.* **74**, 458 (1995).
12. S. V. Kravchenko, D. Simonian, M. P. Sarachik, W. Mason, J. E. Furneaux, *ibid.* **77**, 4938 (1996); Y. Hainein *et al.*, *ibid.* **80**, 1288 (1998).
13. J. P. Eisenstein, L. N. Pfeiffer, K. W. West, *ibid.* **68**, 674 (1992).
14. L. S. Levitov, personal communication; see also V. M. Bedanov and F. M. Peeters, *Phys. Rev. B* **49**, 2667 (1994); R. Egger, W. Hausler, C. H. Mak, H. Grabert, *cond-mat/9903111*.
15. Y. Wan, G. Ortiz, P. Phillips, *Phys. Rev. Lett.* **75** 2879 (1995); M. E. Raikh and L. I. Glazman, *ibid.* **77**, 1354 (1996); A. A. Koulakov and B. I. Shklovskii *Phys. Rev. B* **57**, 2352 (1998); D. L. Miller, *cond-mat/9808103*.
16. Supported by the Office of Naval Research, the Packard Foundation, the National Science Foundation DMR, the Massachusetts Institute of Technology Center for Materials Science and Engineering, and JSEP. We thank L. S. Levitov, M. A. Kastner, and P. A. Lee for illuminating discussions.

5 March 1999; accepted 22 June 1999

# Fault Slip Rates at Depth from Recurrence Intervals of Repeating Microearthquakes

Robert M. Nadeau and Thomas V. McEvilly

Unique attributes in sequences of recurring, similar microearthquakes at Parkfield, California, provide a means for inferring slip rate at depth throughout the active fault surface from the time intervals between sequence events. Application of the method using an 11-year microseismicity record revealed systematic spatial and temporal changes in the slip rate that were synchronous with earthquake activity and other independent measures of fault-zone slip. If this phenomenon is found to be generally common behavior in active faults, it forms the basis for a method to monitor the changing strain field throughout a seismogenic fault zone.

Microearthquake data since 1987 at Parkfield, California, include more than 6000 small events (moment magnitudes in the range of  $-1$  to  $5$ ) along a heavily instrumented segment of the San Andreas fault (1). An organized mode of seismic fault slip was detected by the borehole seismographic network there (2). Most ongoing seismicity can be organized in space and time into about 300 small clusters of microearthquake activity within the fault zone. Most clusters contain sequences of as many as 20 similar, regularly occurring, ("characteristic") microearthquakes (Fig. 1) identified by waveform cross-correlation coefficients  $>0.98$  between pairs of events. The sequences appear to represent repeating slip on adjacent but nonoverlapping patches  $<20$  m wide. More than 99% of the fault surface appears to be slipping without detectable earthquakes. Time intervals between characteristic microearthquakes range from a few months to a few years and scale with event size.

The measured seismic moment-release rate in repeating sequences has been combined with the geodetically determined tectonic loading rate to estimate earthquake source parameters that follow simple scaling relations and describe a fault that is locally strong (kilobar-range stress drops at dimensions of  $<100$  m) but weak at the 10- to 20-km crustal scale of larger earthquakes (3). In this model the clusters define local strength concentrations, or asperities, within the fault zone. We view the recurrence rates

in repeating sequences as indicators of the rate of fault slip at depth (4).

A period of increased earthquake activity began in October 1992 and included the four largest events that occurred since 1987 (magnitudes 4.2, 4.6, 4.7, and 5.0). These earthquakes with their aftershock sequences produced a transient slip on a 25 km<sup>2</sup> strip that

includes the hypocenter of the most recent magnitude 6 earthquake at Parkfield. Summing moments over the total area, the relation  $M = GAs$  among scalar seismic moment ( $M$ ), shear modulus at the fault ( $G$ ), slip area ( $A$ ), and fault slip ( $s$ ) yields an average slip over the strip of 10 to 20 cm for the sequence, consistent with values obtained by deconvolution of locally recorded accelerograms (5). Other deformation-related changes were reported during this period of activity (6, 7).

Changes in previously stable recurrence rates for many repeating sequences began in 1992. This apparent connection between the localized slip in the large earthquakes and the recurrence rates throughout the fault zone motivated our study of recurrence changes and fault slip rate. We identified 160 repeating sequences containing three or more events for a total of 1004 individual microearthquakes, and 844 recurrence interval times. To characterize variability, we computed  $M$  from the observed waveforms for each earthquake and measured the recurrence interval,  $T$ , for every pair of time-adjacent events in a sequence. These two parameters were averaged for each of the sequences to normalize the  $M$  and  $T$  values (Fig.

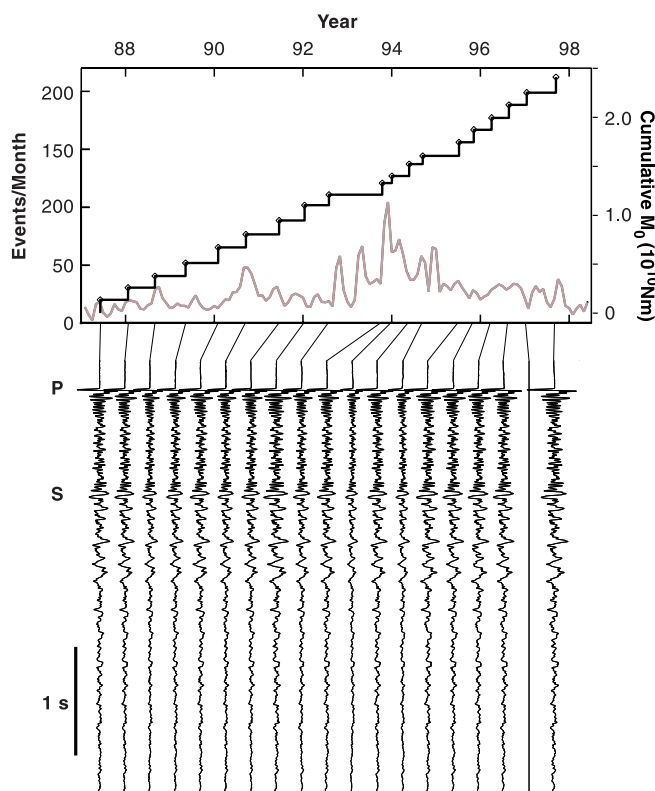


Fig. 1. The upper panel shows the cumulative seismic moment for a sequence of similar microearthquakes (right) and the rate of total seismicity for Parkfield. The lower panel shows example vertical component seismograms for the sequence from borehole station VCA (inoperative for event 18).

Earth Sciences Division, Lawrence Berkeley National Laboratory, and Berkeley Seismological Laboratory, University of California, Berkeley, CA 94720, USA.